JOURNAL OF MATERIALS SCIENCE 31 (1996) 6645–6652

Equilibrium and non-equilibrium intermetallic phases in Al–Fe and Al–Fe–Si Alloys

Á. GRIGER, V. STEFÁNIAY
Aluterv-Fki, Hungalu Engineering and Development Centre, H-1502, PO Box 308, Budapest

The formation of stable and metastable AlFe and AlFeSi intermetallic phases were investigated as a function of their emerging conditions. In the binary system the forming regions of the AlFe intermetallic phases were given as the function of the Fe content and the cooling rate. The transformation of non-equilibrium phases occurs to give the Al_6Fe compound $< 400\,^{\circ}C$, while $> 400\,^{\circ}C$ the Al_3Fe intermetallic phase appears. In the ternary system it is established that formation of the equilibrium phase belonging to a certain phase field is replaced by the non-equilibrium phase forming of the equilibrium phases existing in the "higher" phase region. The thermostability of cubic α-AlFeSi is lower the further its emerging condition from the equilibrium states.

1. Introduction

The solid solubility of Fe in Al is very low (< 0.05 mol %), therefore most of the Fe content, in combination with Al and other elements, appears as intermetallic phases. In the pure binary Al–Fe system, with < 42 mol % Fe content, besides the α-Al solid solution the θ-phase, or Al_3Fe ($Al_{13}Fe_4$) [1], exists as single equilibrium phase (Fig. 1). The θ-phase can appear as a primary crystallized compound or as an eutectic-forming phase depending on the Fe content and the cooling conditions. During non-equilibrium solidification, formation of the equilibrium θ-phase is suppressed by the formation of the non-equilibrium compounds Al_6Fe [2], Al_mFe [3], Al_xFe [4], Al_9Fe_2 [5] and some not properly established phases [6–8]. The type of metastable phase formed is controlled primarily by the melt composition and the local cooling rate.

1.1. Hypoeutectic Al–Fe system

The hypoeutectic alloys prepared at solidification rates $< 10^3\,^{\circ}C\,s^{-1}$ were mainly investigated. In (commercial purity) hypoeutectic AlFe alloys solidified with cooling rates characteristic to the d.c. or strip casting, where the content of possible impurities can be comparable with the quantity of the Fe, some quasi-binary AlFe(X) metastable phases (Al_9Fe_2, Al_xFe) stabilized by impurities, can exist with the equilibrium θ-phase and two non-equilibrium phases (Al_6Fe, Al_mFe). At higher solidification rates (10^3–$10^7\,^{\circ}C\,s^{-1}$) there is neither authentic characterization of the microstructure of hypoeutectic Al–Fe alloys or proper identification of the phases formed under very fast cooling conditions.

1.2. Hypereutectic Al–Fe system

To manufacture hypereutectic Al–Fe alloys with compositions ranging from 2 to 12 mol % Fe content, the conventional casting processes (e.g. d.c. strip or mould casting) are not generally favoured. At the same time, the properties of the Al–Fe alloys of hypereutectic composition solidified during fast cooling are very important from the point of view of industrial practice. The main preparation methods of the Al–Fe alloys of 3.5–12 mol % Fe contents are melt-spun, the splat-quenching technique or gas atomization. These methods cover a range of cooling rates from 10^3 to $10^6\,^{\circ}C\,s^{-1}$, but under extreme conditions the cooling rate can exceed $10^7\,^{\circ}C\,s^{-1}$.

For the sake of improvement of the thermomechanical properties of the rapidly solidified (RS) Al alloys, the quantity of Fe can be increased up to 8–10 mol %. Above this concentration favourable properties do not develop while the ductility drastically decreases.

In the case of rapid solidification, the eutectic point shifts to higher values of Fe content. The eutectic has a very fine structure and the primary phases formed at high cooling rates also have very small particle sizes. In the range of solidification rates of 10^3–$10^5\,^{\circ}C\,s^{-1}$, most authors [6, 7, 9–11] identified firstly the Al_6Fe phase as the major crystalline compound in the eutectic, or as primary intermetallic phase, but the presence of Al_mFe particles was also established [8, 12, 13]. These metastable phases form in the RS hypereutectic system, in which the effect of impurities can be neglected as compared to that of the Fe. At $> 10^7\,^{\circ}C\,s^{-1}$ cooling rates, at relatively high Fe contents, supersaturated solid solutions appear only in the binary Al–Fe RS alloys [14, 15].

1.3. Al–Fe–Si ternary system

In the presence of Si the distribution of Fe is somewhat modified because Si affects its solubility. Because only a small part of the Fe and Si contents are in solid solution, their major form is of binary and/or ternary

0022–2461

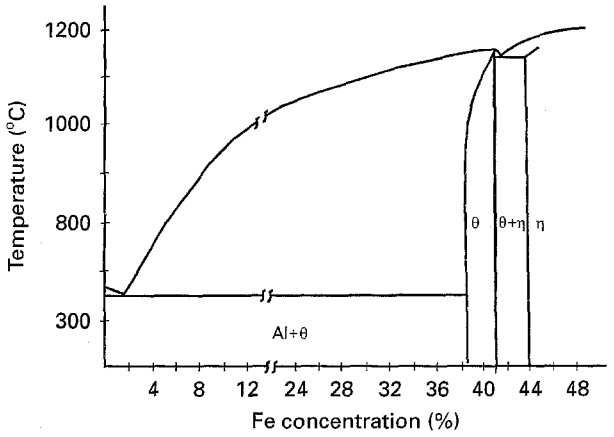

Figure 1 Equilibrium phase diagram of the Al–Fe system.

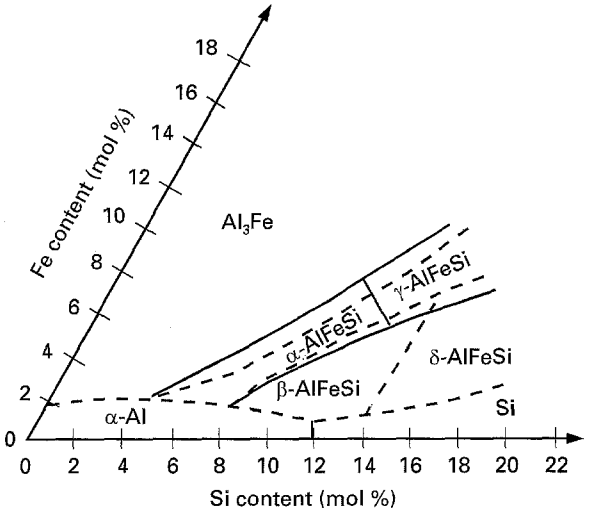

Figure 2 Liquidus surface of the Al–Fe–Si system [16, 18].

intermetallic phases. In high purity alloys with compositions near to the Al corner of the Al–Fe–Si system, in the α-region the hexagonal α-AlFeSi crystallizes (Fig. 2). Cubic metastable α-AlFeSi forms if other elements or impurities are also present [16, 17]. However, Phillips [18] and Armand [19] established that, in this composition range, cubic α-AlFeSi forms in preference to the hexagonal phase. In ternary alloys with their composition in the θ-phase region during non-equilibrium solidification, metastable cubic α-AlFeSi crystallizes instead of θ-AlFe, which grows slowly from the liquid. Iglessis *et al.* [20] determined the critical cooling rate as 3.3 $°C s^{-1}$, above it the cubic α-AlFeSi forms instead of the equilibrium θ-AlFe.

The objective of the present investigation was to characterize the non-equilibrium microstructure of high purity Al–Fe and Al–Fe–Si alloys containing Fe and Si in the 0.25–10 mol % range, which emerged during rapid solidification and mechanical alloying. With cooling rates of 1–10^5 $°C s^{-1}$, as well as during the mechanical alloying process, the dominant primary AlFe and AlFeSi intermetallic phases formed under non-equilibrium conditions were identified and their thermostability was determined. The variation of solid solution contents as a function of Fe content and cooling rate, as well as in the function of the mechanical alloying (milling) time, was also determined.

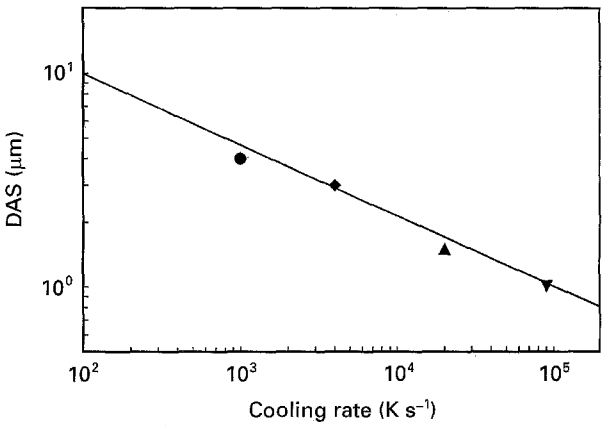

Figure 3 Relationship between the powder size and cooling rate. Particle size (μm): ●, 315–500; ◆, 160–200; ▲, 100–125; ▼, 63–71.

During heat treatments the evolution of the microstructures of alloys with non-equilibrium states was also studied.

2. Experimental procedure

Different Al–Fe and Al–Fe–Si alloys with Fe and Si contents in the 0.2–10 and 0.2–12 mol % ranges, respectively, were prepared on a 99.99% Al basis. The cooling rate of $< 1 °C s^{-1}$ was achieved by casting into an Fe mould with a large heat capacity; the range of 1–500 $°C s^{-1}$ was realized by casting into water-cooled Cu moulds with 30, 8 and 3 mm diameters, and by common d.c. casting. Solidification rates $> 10^3 °C s^{-1}$ were produced by Ar gas atomization and melt-spinning methods. With the separation of the powder into size fractions by sieving, the actual solidification rates of the fractions were estimated by means of the empirical relationship between the secondary dendrite arm spacing and the solidification time suggested by Matyja *et al.* [21] (Fig. 3).

AlFe8, AlFe30Si8 and AlFe12Si2 alloys of non-equilibrium states were prepared by the mechanical alloying (MA) route.

Heat treatment of the samples was carried out between 300 and 625 °C for 1–24 h. Some samples were also prepared by hot extrusion at 380–400 °C.

X-ray powder diffraction (XRD) measurements were performed to identify the intermetallic crystalline compounds formed during solidification and the MA process, as well as during heat treatments. The solid solution content was estimated from electrical resistivity measurements performed by a standard potentiometric method and by means of Mössbauer spectroscopy (MS). The phase morphology was studied by transmission and scanning electron microscopies (TEM and SEM, respectively).

3. Results and discussion

3.1. Phase formation during solidification and mechanical alloying

In as-cast states the dominant intermetallic phases identified by XRD can be seen in Table I as functions of the solidification rate and Fe concentration of the

TABLE I Formation of AlFe intermetallic phases as a function of Fe content and cooling rate

Fe content (%)	Cooling rate ($°C s^{-1}$)							
	1	10	100	500	$> 10^3$	10^4	10^5	$> 10^5$
0.25	A_6	A_6	A_6	A_m	–	–	–	–
0.50	A_3	A_6	A_6	A_m	n.d.	–	–	n.d.
1.0	–	–	A_6	–	–	–	–	–
1.8	A_3	A_6	A_6	A_m	–	–	–	–
3.2	–	A_3	A_6, A_m	$A_m(A_6)$	–	A_m	–	A_m
5.5	–	–	–	–	A_6	–	–	–
6.8	–	A_3	A_3	$A_6(A_m)$	–	$A_m(A_6)$	A_m	A_m
9.2	–	A_3	A_3	A_3	–	$A_6(A_m)$	A_m	A_m

A_3, Al_3Fe; A_6, Al_6Fe; A_m, Al_mFe; n.d., not detected; –, not measured.

TABLE II Variation of Fe content in solid solution as a function of Fe concentration of alloys and cooling rate

Cooling rate ($°C s^{-1}$)	Fe concentration (%)				
	0.5	1.8	3.2	6.3	9.2
1	0.041	0.053	0.058	0.076	0.087
10	0.050	0.075	0.064	0.090	0.102
500	0.059	0.112	0.101	0.114	0.104
1000	0.19	–	–	0.26	–

materials. The solid solution contents can be found in Table II.

In the melt-spun ribbon with 0.5 mol % Fe content, which solidified with an estimated cooling rate of 10^3 $°C s^{-1}$, globular intermetallic phases with particle sizes 0.1–0.2 μm can be seen at the cell boundaries and inside the cells (Fig. 4a). In the RS powder samples with cooling rates $> 10^5$ $°C s^{-1}$ no considerable precipitation could be detected either at the cell boundaries or inside the cells (Fig. 4b). In the hypereutectic alloys with 3.9, 5.5, 6.8 and 9.2 mol % Fe contents, Al_mFe, Al_6Fe and Al_3Fe intermetallic compounds were formed as the main components depending on the cooling rate ($10–10^5$ $°C s^{-1}$) and composition (Table I).

At the solidification rate of 500 $°C s^{-1}$ in the alloy with 3.9 mol % Fe content, primary Al_mFe particles and Al–Al_mFe eutectic can be found (Fig. 5). In the sample with 6.8 mol % Fe content, the Al_6Fe compound exists as primary phase but at 9.2 mol % Fe content star-like Al_3Fe particles form, with sizes < 10 μm (Fig. 6). At higher Fe contents and lower cooling rates (< 500 $°C s^{-1}$), Al_3Fe intermetallic phase and Al–Al_3Fe eutectic form as primary phases. The size of Al_3Fe particles increases up to 100 μm with decreasing cooling rates.

The supersaturated solute Fe content increases with cooling rate and the Fe concentration of the alloys, but it does not remarkably exceed the equilibrium

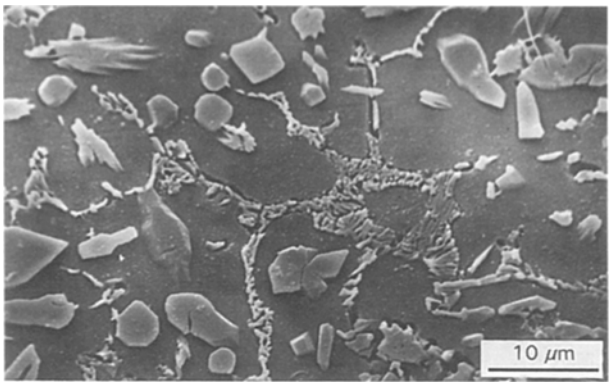

Figure 5 Primary Al_mFe crystals and Al–Al_mFe eutectic (3.9 mol % Fe; cooling rate, 500 $°C s^{-1}$).

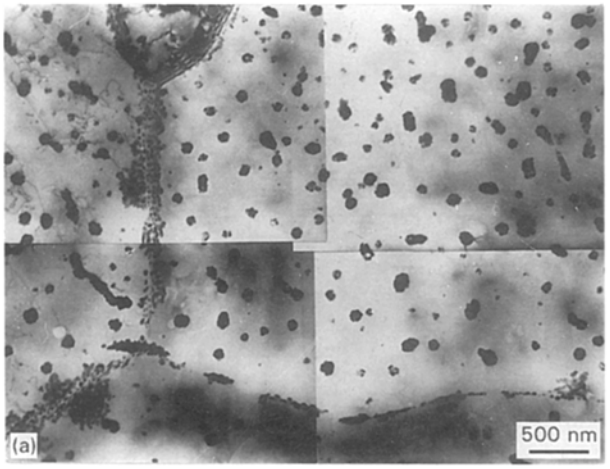

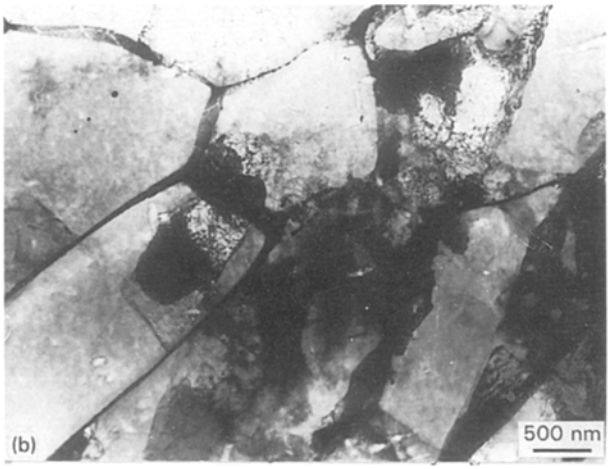

Figure 4 Microstructure in the hypereutectic Al–Fe alloy with different cooling rates. (a) Melt-spun ribbon (10^3 $°C s^{-1}$) ; (b) gas-atomized powder (10^5 $°C s^{-1}$).

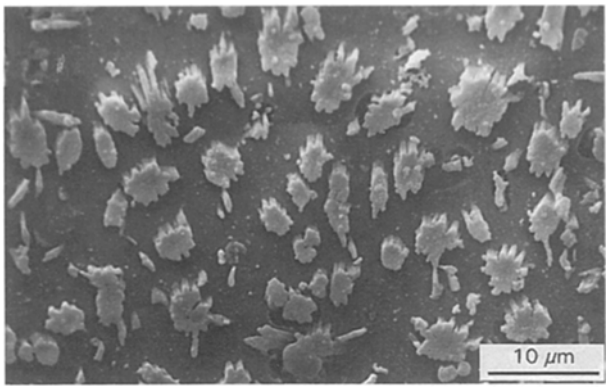

Figure 6 Tenfold star-like twinned Al_3Fe primary crystals (9.2 mol % Fe; cooling rate, 500 °C s^{-1}).

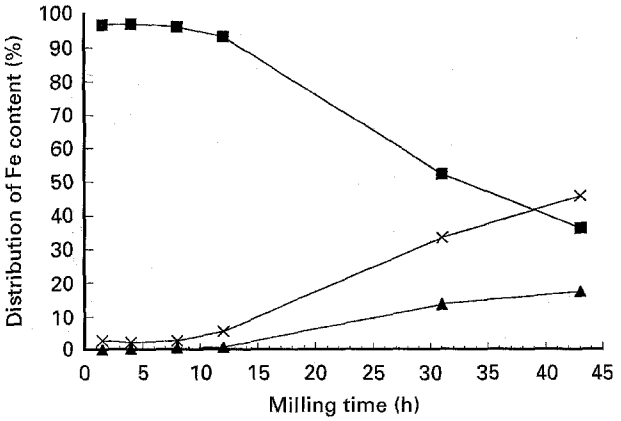

Figure 7 Distribution of Fe content in AlFe phases as a function of milling time. ■, α-Fe; ▲, Fe in SSS; ×, Al–Fe cluster.

value (Table II). This means that the Fe in the alloys investigated can mostly be found in intermetallic phases. It should be mentioned that in the hypereutectic range a further increase in the Fe content in solid solution as a function of the total Fe content of the alloys can hardly be observed.

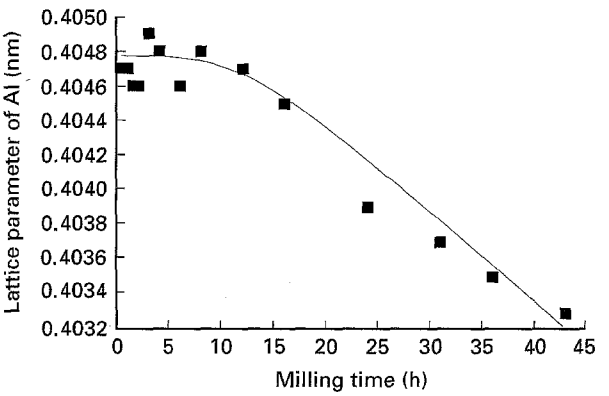

Figure 8 Variation of the lattice parameters of Al as a function of milling time.

In the case of MA AlFe8 alloy, the solid solution content increases with the milling time (alloying time) [22]. After 12 h the α-Fe content drastically decreases and metastable AlFe clusters form, and the Fe content of the α-Al solid solution increases gradually, which could be also followed by the shifts of the Al lines in the XRD patterns (Figs 7 and 8).

The results of XRD phase analysis obtained on the Al–Fe–Si alloys solidified with different cooling conditions can be seen in Table III. On the basis of their composition, the investigated samples could be located in the α-Al solid solution, θ-AlFe, α-AlFeSi and the β-AlFeSi regions of the equilibrium phase diagram. In our case, the cooling rate applied was already too fast for the formation of the equilibrium intermetallic phases during solidification. In the MA Al–Fe–Si alloys no crystalline intermetallic phases appeared, however, the Si and Fe lines disappeared in the XRD patterns and the Al lines significantly broadened. According to TEM investigations, these alloys possessed a very homogenous nanocrystalline structure.

TABLE III Formation of AlFeSi intermetallic phases as a function of Fe and Si contents and cooling rate

Phase field	Composition (%)			Cooling rate (°C s^{-1})					
	Fe	Si	Fe/Si	< 10	100	500	1000	10^4	10^5
α-Al	0.9	0.25	3.6	$A_3(A_6)$	–	–	–	–	–
	0.5	0.2	2.5	α_c	α_c	α_c	–	–	α_c
	0.5	0.5	1.0	α_c	–	–	–	–	–
	0.2	0.2	1.0	α_c	–	–	–	–	–
	0.5	1.0	0.5	β	–	n.d.		–	n.d.
Θ	10.9	1.7	6.4	–	–	–	A_3 + Si	$\alpha_c + \alpha_H$	α_c
	10.0	2.0	5.0	–	$\alpha_c + A_3$	α_c	–	–	–
	10.4	2.2	4.7	–	$\alpha_c + A_3$	$\alpha_c + A_3$	$\alpha_c + (\alpha_H)$	–	–
	7.6	2.1	3.5	–	–	–	–	–	α_c
	8.6	2.5	3.4	$A_3 + \alpha_c$	–	–	–	–	–
	7.5	2.4	3.0	–	$\alpha_c + A_3$	$\alpha_c + A_3$	α_c	–	–
	3.3	1.1	3.0	$A_3 + \alpha_c$	–	–		–	–
	5.2	1.9	2.7	$\alpha_c + A_3$	–	–	–	–	–
	4.3	5.0	0.8	$\alpha_H + \alpha_c$	–	–		–	–
α	7.0	13.6	0.5	β + Si	–	–		–	–
	5.0	9.7	0.5	β + Si	–	–	–	–	–
	5.0	12.0	0.4	–	–	–	–	δ + β + Si	Si + δ + β
β	1.5	9.2	0.2	β + Si	–	–	–	–	–

α, β and δ, α-, β- and δ-AlFeSi, respectively; $_c$, cubic; $_H$, hexagonal.

TABLE IV Phase transformation in RS AlFe alloys

As-cast condition			Heat treatment (Exposure 1–3 h) Temperature (°C)						
Fe (%)	Cooling rate ($°C s^{-1}$)	Phases	300	400	450	500	580	605	625
0.5	10^5	n.d.	–	A_6	–	–	A_6	–	–
0.5	10^3	n.d.	–	A_6	–	–	A_3	–	–
0.5	500	A_m	–	A_m, A_6	–	–	–	–	–
0.5	10	A_6	–	–	A_6	–	$A_6(A_3)$	$A_6(A_3)$	A_3
1.8	500	A_m	–	–	A_6, A_m	–	–	–	–
3.9	10^5	A_m	A_m	A_m	–	A_3	A_3	–	–
5.5	10^3	A_6	A_6	$A_6, (A_3)$	–	–	–	A_3, A_6	–
6.8	10^5	A_m	A_m	A_m	–	A_3	A_3	–	–
9.2	10^5	A_m	A_m	A_m	–	A_3	A_3	–	–

3.2. Phase transformation of AlFe and AlFeSi phases (heat-treated condition)

The binary alloys containing different AlFe phases formed at different cooling rates in the $< 1 - 10^5\ °C s^{-1}$ range were heat treated at different temperatures for several different exposure times. The transformed phases identified by XRD are summarized in Table IV.

In the hypoeutectic d.c.-cast alloy with 0.5 mol % Fe content the transformation of the metastable Al_6Fe phase begins 1 h after heat treatment commenced at 580 °C. Acicular Al_3Fe particles precipitate from the supersaturated solid solution (Fig. 9). The full transformation of the Al_6Fe intermetallic phase takes place > 580 °C after 16 h, below this temperature the dissolution process of the Al_6Fe takes a long time (> 24 h) [23]. The transformation of $Al_mFe \rightarrow Al_3Fe$ starts > 400 °C after 2 h. The submicrometre particles formed under fast cooling in RS powder and melt-spun ribbon with 0.5 mol % Fe content become detectable as Al_6Fe at 400 °C after 2 h. In the hypereutectic alloys the transformation processes of the Al_6Fe and Al_mFe alloys correspond to those of the Al_mFe and Al_6Fe alloys in hypoeutectic alloys, respectively.

In the MA AlFe8 alloy the nanocrystalline α-Fe, AlFe cluster and the non-equilibrium α-Al solid solution content transformed into a well crystallized Al_6Fe phase during heat treatment for 4 h at 300 and 400 °C,

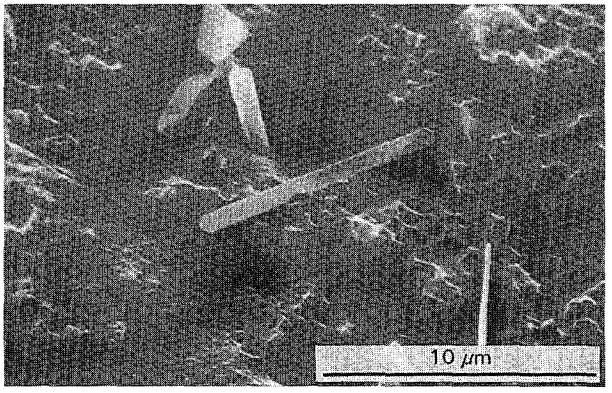

Figure 9 Al_3Fe particles precipitated from supersaturated solid solution.

while > 500 °C the Al_3Fe intermetallic phase formed during 1 h. During hot extrusion (at 380–400 °C) the RS powder material suffered a strong thermomechanical treatment. In the rods hot extruded from RS powder of 0.5 mol % Fe content the crystalline Al_6Fe phase could be identified, while in the RS powder the AlFe compounds were not detected by XRD. In the hot-extruded hypereutectic alloys a huge amount of fine globular particles, 0.2–0.5 μm in size, and some non-transformed primary particles could be found. In these samples the quantity of the original, poorly crystallized AlFe phases decreased, and well developed Al_6Fe crystals and a small amount of Al_3Fe compound appeared.

In the alloy with 0.5 mol % Fe content, as well as 0.2 and 1 mol % Si content, the crystal structure of the primary phases formed under non-equilibrium conditions did not change during heat treatment between 450 and 575 °C for 16 h. The cubic α-AlFeSi → θ-AlFe phase transformation did not take place completely even during heat treatment for 24 h at 605 °C; a small amount of α-AlFeSi phase could be still detected. The equilibrium state was approached by consecutive heat treatments at 630 °C. The particles of cubic α-AlFeSi intermetallic phase coagulate first and then dissolve gradually. At the same time, the nuclei of θ-AlFe intermetallic compound appear, which grow as acicular crystallites and develop further to particles with irregular shapes (Fig. 10a–c). In alloys with higher Si contents, during the heat treatments the β-AlFeSi alloy formed under different cooling conditions did not transform into another phase below 620 °C, but its morphology changed slightly (Fig. 11a–c). Above 620 °C the transformation of β-AlFeSi to hexagonal α-AlFeSi occurred according to the phase diagram.

In the RS material with 11 mol % Fe and 2 mol % Si contents the non-equilibrium primary phases, the cubic α-AlFeSi and θ-AlFe, formed at cooling rates $> 10^5$ and at 10^3, respectively. The non-equilibrium poorly crystallized cubic α-AlFeSi and θ-AlFe intermetallic phases transformed into crystalline cubic α-AlFeSi at 430 °C in under 24 h and into hexagonal α-AlFeSi intermetallic compound at 530 °C after 24 h (Table V). In the MA AlFe8Si2 alloy, cubic α-AlFeSi phase formed from the nanocrystalline Al containing high Si and Fe contents in solid solution during heat

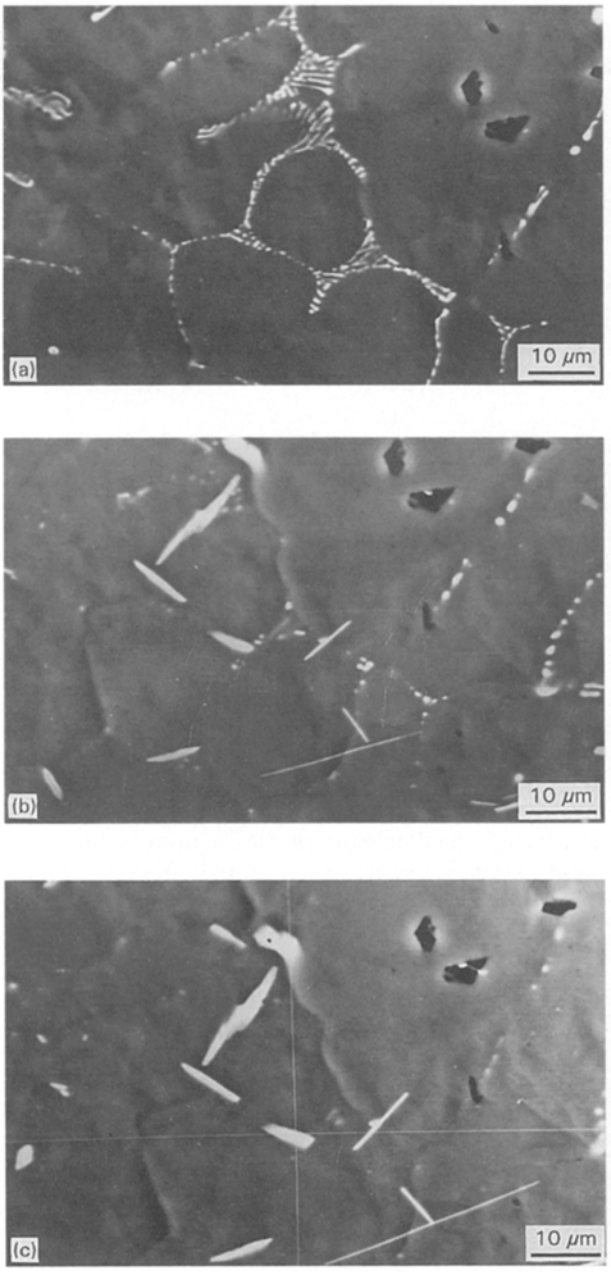

Figure 10 Transformation of the α_c-AlFeSi intermetallic phase at 630 °C. (a) As-cast condition; (b) after 4 min; (c) after 8 min.

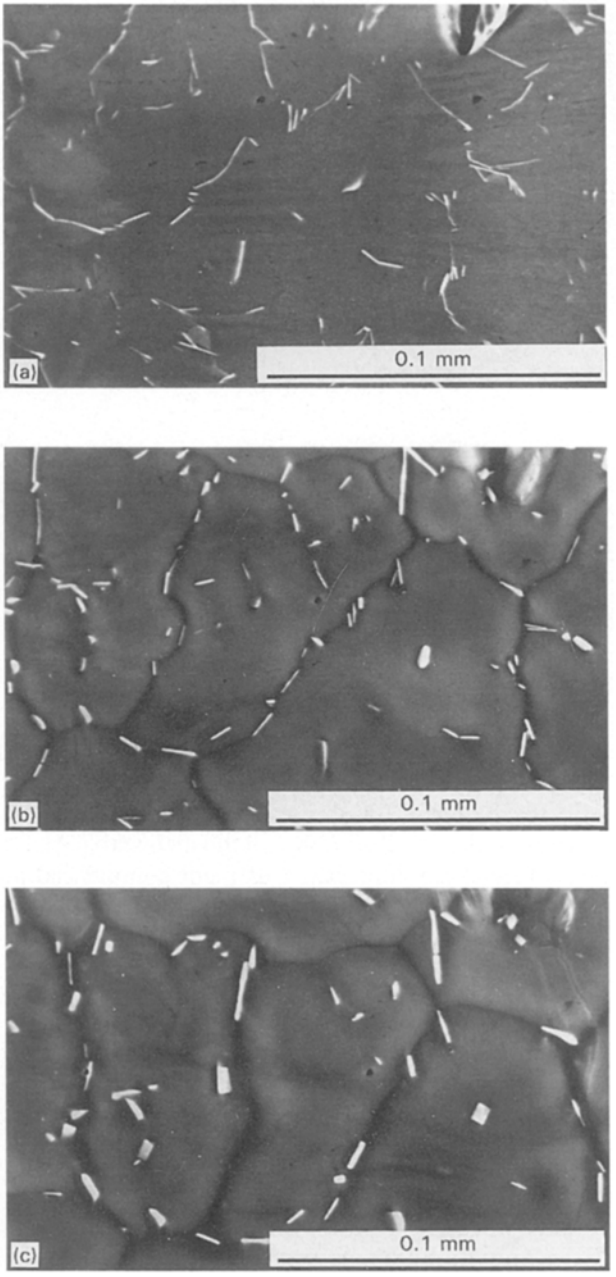

Figure 11 Morphological changes of the β-AlFeSi intermetallic phase at 620 °C. (a) As-cast condition; (b) after 2 min; (c) after 8 min.

treatments at 300 and 430 °C exposed for 24 h. At 530 °C, during 1 h, heat treatment also resulted in cubic α-AlFeSi, while after 24 h hexagonal α-AlFeSi could be identified (Table VI). These results are similar to that of RS materials with the same composition. In the MA AlFeSi alloy (AlFe30Si6) with a high alloying concentration the phase transformation was rather different from that which took place in the MA AlFeSi alloy with a lower alloying content. At 300 °C during 24 h the nanocrystalline structure of the Al matrix remained and a small amount of cubic α-AlFeSi phase formed. At 430 and 530 °C, even after 24 h, deformed θ-AlFe and elemental Si developed.

TABLE V Formation and transformation of AlFeSi intermetallic phases in RS alloys

State	Cooling rate (°C s^{-1})		
	10^3	10^4	10^5
As fabricated	$A_3 + Si + Al$	$\alpha_C + Al$	$\alpha_C + Al$
Heat treated			
430 °C for 24 h	$\alpha_C + Al$	$\alpha_C + Al$	$\alpha_C + Al$
530 °C for 24 h	$\alpha_H + Al$	$\alpha_H + Al$	$\alpha_H + Al$

4. Conclusions

From our results and the literature, it can be concluded that in the pure binary Al–Fe system the possible phases emerging exclusively, from the melt are the Al_3Fe, Al_6Fe and Al_mFe compounds, both in the hypo- and hypereutectic systems. As a summary of our results a phase map can be drawn, where the forming and existence range of different AlFe phases are determined as a function of the composition and the cooling rate (Fig. 12) [24]. On Fig. 12 the values of different authors are also presented. Near to the Al

TABLE VI Transformation of AlFeSi intermetallic phases in MA alloys

Samples	As fabricated	Heat treated					
		300 °C		430 °C		530 °C	
		1 h	24 h	1 h	24 h	1 h	24 h
AlFeSi82	Nanocry. Al, Si	–	α_c + Al	α_c + Al	α_c + Al	α_c + Al	α_H + Al
AlFe30Si6	Nanocry. Al, Fe, Si	Nanocry. Al, Fe, Si	Nanocry. Al, Fe, Si + α_c	Def. A_3 + Si	A_3 + Si	Def. A_3 + Si	A_3 + Si

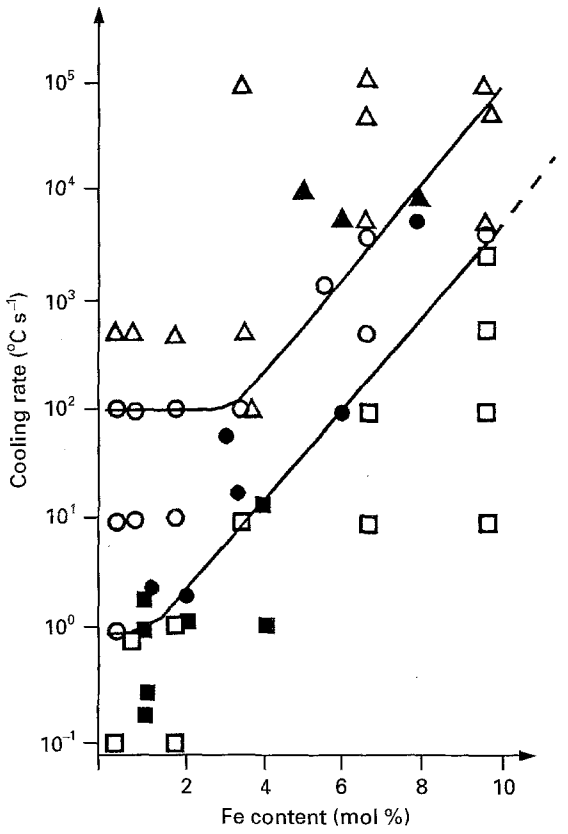

Figure 12 Forming range of the AlFe intermetallic phases as a function of Fe content and cooling rate □, ■, Al_3Fe; ○, ●, Al_6Fe; △, ▲, Al_mFe. (■, ● and ▲, data from Refs [7, 8, 11, 13, 25–27]).

corner, the primary AlFe constituent can be predicted by means of the relationship suggested by Miki *et al.* [3]. This relationship gives the order of magnitude of the solidification rate in the case of a given phase formation at the hypoeutectic composition. In this narrow range of Fe contents our results show very good agreement with Miki *et al.* [3].

It can be seen that below the equilibrium and the non-equilibrium eutectic points (Fe < 1.8 and < 3.5 %, respectively), the formation of the metastable Al_6Fe and Al_mFe intermetallic compounds depends only on the cooling rate and not on the Fe content. Above these Fe concentrations, the higher the Fe content the higher the solidification rate needed for formation of the Al_6Fe and the Al_mFe metastable phases. By increasing the solidification rate, the Al_3Fe equilibrium phase is replaced first by Al_6Fe and at higher rates by Al_mFe intermetallic compounds.

The thermostability of the individual metastable phases is independent of the circumstances of their formation. Above 400 °C the transformation of the metastable phases leading to the equilibrium state seems to be $Al_mFe \rightarrow Al_3Fe$ and $Al_6Fe \rightarrow Al_3Fe$. During heat treatments the metastable phases Al_mFe and Al_6Fe dissolve and rod-like Al_3Fe precipitates are formed by heterogeneous nucleation because of the good lattice matching, in certain directions, with the parent matrix. Below 400 °C clusters and/or quasi-amorphous, nanocrystalline intermetallic phases formed under non-equilibrium conditions (during mechanical alloying or rapid solidification) transform into metastable Al_6Fe. Similarly, in the rods hot extruded (at 380–400 °C) from RS powder containing practically all Al_mFe phase, the Al_6Fe phase could be found.

Hot extrusion is a relatively complicated process since during pressing under increased pressure a steadily recovered deformed structure forms at an elevated temperature. In this case, as an effect of the deformed structure and the relatively low temperature, the Al_mFe compound might transform directly into Al_6Fe. A probable explanation could be that during heat treatment the Fe content of the Al–Fe clusters, of the quasi-amorphous AlFe compounds (in MA alloys) and of the Al_mFe with a deteriorated structure (in RS materials) goes into solid solution and immediately precipitates as Al_6Fe due to the applied low temperature (< 400 °C). This means that in the binary system there is a relatively stable metastable state, where the (quasi-) equilibrium phase is the Al_6Fe metastable intermetallic phase instead of the Al_3Fe compound. The sequence of stability of AlFe intermetallic phases is Al_mFe and Al_6Fe (and Al_3Fe).

In the ternary system the phase formation was controlled firstly by the Fe:Si ratio. But it can be established that with increasing cooling rates the formation of the equilibrium phase belonging to a given phase field is suppressed by the non-equilibrium formation of other phases which are equilibrium phases in the "higher" phase regions.

It is proved that the formation of the cubic α-AlFeSi is possible without the effect of other stabilizer elements in Al–Fe–Si alloys with higher Fe (≫1 mol %) and Si (≫1 mol %) contents. In the ternary system the phase transformation is a slower process than in the binary one. It takes place only at high temperatures (> 530 °C) during long heat treatments. Similar to the

binary system, at heat treatments of lower temperatures, quasi-equilibrium states can exist where metastable phases replace the equilibrium ones. The cubic α-AlFeSi intermetallic phase formed in Al–Fe–Si alloys with high Fe and Si contents under non-equilibrium conditions is stable only up to ca. 500 °C. Above this temperature the transformation occurs into hexagonal α-AlFeSi or θ-AlFe depending on the Fe:Si ratio. It means that the transformation rate of the metastable cubic α-AlFeSi depends on its emerging conditions.

Acknowledgement

This publication is based on the work sponsored by the OTKA Fund under project number 278.

References

1. A. GRIGER, V. STEFÁNIAY and T. TURMEZEY, *Z. Metallkde* **77** (1986) 30.
2. L. K. WALFORD, *Acta Crystallogr.* **18** (1965) 287.
3. I. MIKI, H. KOSUGE and K. NAGAHAMA, *J. Jan. Inst. Met.* **25** (1975) 1.
4. R. M. K. YOUNG and T. W. CLYNE, *Scripta Metall.* **15** (1981) 1211.
5. C. J. SIMENSEN and R. VALLESAMY, *Z. Metallkde* **68** (1977) 428.
6. D. SHECHTMAN and L. J. SWARTZENDRUBER, *Mater. Res. Soc. Symp. Proc.* **19** (1983) 265 (published by Elsevier).
7. D. J. SKINNER, K. OKAZAKI and C. M. ADAM, "Rapid Solidified Powder Aluminium Alloys" ASTM STP 890, edited by M. E. Fine and E. A. Starke Jr (American Society for Testing Materials, PA, USA, 1986) p. 211.
8. M. CHANDRASEKARAN, Y. P. LIN, R. VINCENT and G. STANIEK, *Scripta Met.* **22** (1988) 797.
9. H. JONES, *Mater. Sci. Engng.* **5** (1969) 1.
10. M. H. BURDEN and H. JONES, *Metallography* **3** (1970) 307.
11. W. J. BOETTINGER, L. BENDERSKY and J. G. EARLY, *Metall. Trans. A* **17A** (1986) 781.
12. M. YOKOTA, T. UEDA, H. KURODA and K. SHOJI, *J. Jan. Soc. Powder and Powder Met.* **34** (1987) 254.
13. P. RENAUT and G. LAPASSET, *Rapid Quenched Metals* (1985) 815.
14. P. FURRER and H. WARLIMONT, *Z. Metallkde* **64** (1973) 236.
15. A. KAMIO, H. TEZUKA and T. SATO, *J. Jan. Inst. Light Metals* **36** (1968) 72.
16. D. MUNSON, *J. Inst. Metals* **95** (1976) 217.
17. C. Y. SUN and L. F. MONDOLFO, *ibid.* **95** (1976) 384.
18. H. W. L. PHILLIPS, "Annotated Equilibrium Diagrams of some Aluminium Alloys" (monograph 25) 1959.
19. M. ARMAND, Congrés International de i Aluminium (Paris, 1954) *Paris Revue de i Aluminium* **1** (1955) 305.
20. J. IGLESSIS, C. FRANCZ and M. GANTOIS, *Mém. Sci. Rev. Mét.* **74** (1978) 93.
21. H. MATYJA, B. C. GIESSEN and N. J. GRANT, *J. Inst. Metals.* **96** (1968) 30.
22. E. KUZMANN, A. VÉRTES, Á. GRIGER, and V. STEFÁNIAY, in ICAME International Conference on the Application of Mössbauer Effect, August 1993 (Vancouver, Hyperfine Interactions) in press.
23. Á. GRIGER, V. STEFÁNIAY and T. TURMEZEY, *Aluminium* **65** (1989) 1049.
24. Á. GRIGER, V. STEFÁNIAY, E. KOVÁCS-CSETÉNYI and T. TURMEZEY, *Key Engng. Mater.* **44 & 45** (1990) 17.
25. L. BACKERUD, *Jernkontorets Ann.* **152** (1968) 109.
26. C. McL. ADAM and L. M. HOGAN, *J. Australian Inst. Metals* **17** (1972) 81.
27. J. STRID, D. A. PORTER and K. E. EASTERLING, *Mater. Sci. Technol.* **1** (1985) 161.

Received 12 October 1994
and accepted 13 February 1996